CHAPTER 2

Theory and Principle

An electron gun in this study is a 1.6-cell BNL type S-band photocathode RF-gun, which was developed at the High Energy Accelerator Research Organization (KEK), Japan [11]. The gun has half-cell and full-cell resonant cavities. During this study, a copper cathode was placed at the center of the rear wall of the half-cell cavity. It produces free electrons via the photoelectric effect. A high power radio-frequency (RF) wave with a frequency of 2856 MHz is transported from a 10-MW klystron through a rectangular waveguide system, which is connected to the RF-gun at the cylindrical wall of the full-cell cavity. The RF wave is fed into the half-cell cavity via a central iris between the two cavities. A solenoid magnet is placed downstream the RF-gun for focusing and compensation of the space-charge effect. Quadrupole magnets are installed in the beam transport line to control the transverse beam size. Characteristics of electron beams produced from the RF-gun depend greatly on the electron distributions in the 6-dimensional phase space. The transverse phase space is related to the electron beam size and emittance. The longitudinal phase space determines the electron beam energy, energy spread and bunch length. Several beam diagnostics are needed in the accelerator system to investigate the electron beam properties. The quadrupole magnet and a fluorescent screen are used to measure the beam emittance. A dipole magnet and a view screen are utilized in the electron beam energy measurement. A Faraday cup is used in the charge measurement. To understand functionalities of the photocathode RF-gun and other elements in the accelerator system, all concerned principles and theory are discussed in this chapter.

2.1 Principle of Photocathode Emission

The first photoelectric emission from metals was studied by Heinrich Hertz in 1887 [12]. Then, Albert Einstein proposed the theory to explain the principle of photoelectric process in 1905. The theory presents the quantization of the light energy and proposes an escape energy of photoelectron, which depends on properties of materials. This energy is known as a work function of the material in present days. The principle of the photoelectric effect is described as following. When photon shines upon a metal, the photon energy is transferred to electrons inside the material surface. If the photon energy is larger than the work function, the excited electron can escape from the metal surface with the kinetic energy (*KE*) of

$$KE = h\nu - \phi, \tag{2.1}$$

where h is the Planck's constant, ν is the frequency of the incident photon and ϕ is the work function of the cathode material. The theory of the photoemission in the photoelectric effect based on the three-step model [13]. The model divides the process into three independent steps. The first step is a photon absorption, which results in electron excitation. The second step is a movement of the excited electron to the surface of cathode. The last step is an emission of the excited electron from the cathode.

The quantum efficiency (*QE*) of the photocathode is introduced to determine the ratio of the number of emitted electrons (n_e) to the number of incident photons (n_p). A standard definition of the quantum efficiency in practical unit is given by [14]

$$QE = \frac{n_e}{n_p} \tag{2.2}$$

Thus, a physical idea of the QE is a probability of a single photon that can generate an emitted electron from the cathode material, which is related to a product of the probability of each step in three-step model.

2.1.1 Three-step Model of Photoemission

In the first step of photoemission, the probability of photon absorption for exciting electron to higher energy state is calculated. The process in this step is almost the same for both metallic and semi-conductor materials. There are two assumptions considered in this step. The first assumption is that all states, which has energy below the Fermi energy (E_F), are filled and the states, which have energy above the Fermi energy, are empty [15]. The second assumption is that every absorbed photons excite electrons in the cathode surface. Thus, the probability depends on the photon energy, a number of electrons in an occupied energy state and a number of available states for the excited electrons. In case of the first assumption, the probability of the incident laser transmission $T(v)$ can be calculated to be

$$T(\nu) = 1 - A(\nu) - R(\nu), \tag{2.3}$$

where $A(v)$ is the probability of the photon absorption in the cathode material and $R(v)$ is the probability of reflection of the incident photon.

For the second assumption, the estimation considers the probability of the excitation of electron from an initial energy state E_0 to a final energy state $E=E_0+hv$. The probability is then proportional to a number of the initial state $N(E_0)$ and a number of the final state $N(E)$, as

$$P(E, hv) \propto N(E_0)N(E) = N(E - hv)N(E)\,. \tag{2.4}$$

The probability is obtained by considering a fraction of the total number of interested states and the total number of possible states, which is

$$\int_{E_F}^{E_F + hv} dE'\, N(E')N(E' - hv)\,. \tag{2.5}$$

At the lower limit of the integration, the states below the Fermi energy state are filled. For the upper limit, all excitation states refer to the states above the Fermi energy state. Thus, the probability of the electron excitation to the final state becomes

$$P(E, hv) = \frac{N(E)N(E - hv)}{\displaystyle\int_{E_F}^{E_F + hv} dE' N(E')N(E' - hv)}\,. \tag{2.6}$$

In the second step, the probability of the excited electron traveling to the cathode surface is calculated. The process in this step differs between metallic and semi-conductor materials. In this study, we concentrate on the metallic material because the photocathode is made of copper. In case of metal, electrons may scatter with electrons, phonons and impurities while they travel to the cathode surface. However, this model considers only the electron-electron scattering process, which makes the excited electron to lose a sufficient energy and cannot escape from the cathode. A lifetime of an excited state $\tau(E)$ is inversely proportional to the electron-electron scattering probability as [16]

$$\tau(E) \propto \frac{1}{S(E)}, \tag{2.7}$$

where *S(E)* is the electron-electron scattering probability. To simplify the assumption, the interaction between the valence electrons and the excited electron is ignored and a probability of the interaction is only a function of a number of the available initial and final energy states. Thus, the total probability of the scattering of an electron with energy *E* by the electron with energy E_0 for all possible energy transition states ΔE is related to

$$S(E,E_0) \propto \int_{E_F-E_0}^{E-E_F} d(\Delta E)N(E_0)N(E_0+\Delta E)N(E-\Delta E), \tag{2.8}$$

where $N(E_0)$ is the number of electron with energy E_0, $N(E_0+\Delta E)$ is the number of empty states with energy $E_0+\Delta E$, $N(E-\Delta E)$ is the number of empty states with energy $E-\Delta E$. The lower limit of the integration in equation (2.8) represents a kinematic limitation, which is $E+E_0 \geq 2E_F$ [14]. Then, equation (2.8) becomes

$$S(E) \propto \int_{2E_F-E}^{E_F} dE_0 \int_{E_F-E_0}^{E-E_F} d(\Delta E)N(E_0)N(E_0+\Delta E)N(E-\Delta E). \tag{2.9}$$

The electron-electron scattering process limits a traveling length of the excited electron in the material, which is represented by the electron-electron scattering length (λ_e). Herein, we assume that the electron velocity is proportional to square root of its kinetic energy, which is taken to be the energy above the Fermi energy. Then, we get $v(E)=\sqrt{E-E_F}$ and the scattering length becomes

$$\lambda_e(E) = v(E)\tau(E) = \frac{\alpha\sqrt{E-E_F}}{\int_{2E_F-E}^{E_F} dE_0 \int_{E_F-E_0}^{E-E_F} d(\Delta E)N(E_0)N(E_0+\Delta E)N(E-\Delta E)}, \tag{2.10}$$

where α is the constant of proportionality. The mean distance that the excited electron travels to reach the cathode surface is related to the photon absorption length (λ_{ph}), which can be calculated from [17]

$$\lambda_{ph} = \frac{\lambda}{4\pi k} \ , \tag{2.11}$$

where λ is the photon wavelength and k is related to the complex part of the refraction index, which is $N = n + ik$. The probability that the electron will escape at the depth d corresponds to e^{-d/λ_e}. Then, the probability per unit length that photon is absorbed by the electron at the depth d is $\lambda_{ph}^{-1} e^{-d/\lambda_{ph}}$. The fraction of electrons, which reach the cathode surface without scattering, can be obtained by integrating the product of these two probabilities and it becomes [14]

$$T(E,v) = \frac{\lambda_e(E)/\lambda_{ph}(v)}{1+(\lambda_e(E)/\lambda_{ph}(v))} \, . \tag{2.12}$$

In the final step, the probability of electrons that reach and escape from the surface is calculated. The motion direction of electrons, which can escape from the cathode surface, must lie within a cone determined by electron energy and work function of the cathode material. An opening angle of the cone (θ) is described by [18]

$$\cos(\theta) = \frac{k_{\perp\min}}{\left|\vec{k}\right|} = \sqrt{\frac{E_T}{E - E_F}}, \tag{2.13}$$

where E_T is the required energy of electron to escape from the cathode surface and $k_{\perp\min}$ refers to the value of transverse component of electron momentum. In case of metal, the required energy equals to the work function of material ($E_T = \phi$). The fraction of total solid angle described the number of electrons, which escape from the cathode surface, is [14]

$$D(E) = \frac{1}{4\pi}\int_0^{\theta} \sin(\theta')d\theta' \int_0^{2\pi} d\varphi = \frac{1}{2}[1-\cos(\theta)] = \frac{1}{2}\left(1 - \sqrt{\frac{E_T}{E - E_F}}\right), \tag{2.14}$$

Then, the QE, which is related to the total probability, corresponds to

$$QE(v) \propto \int_{E_T}^{hv+E_F} P(E)T(E,v)D(E)dE \, . \tag{2.15}$$

In case that the electron energy is very close to the threshold of the emission energy $(E - E_T \ll E_T)$, the probability of electron with energy E escaping from the metal is proportional only to $D(E)$ [14]. Thus, the total QE is proportional to the integral of $D(E)$ over the possible electron energies as

$$QE(v) \propto \int_{E_F+\phi}^{E_F+hv} D(E)dE \, , \tag{2.16}$$

$$QE(v) \propto 2\phi - 2\phi\sqrt{1+\frac{hv-\phi}{\phi}} + (hv-\phi) \, . \tag{2.17}$$

Then, we get

$$QE(v) \propto 2\phi - 2\phi\left(1+\frac{hv-\phi}{2\phi}-\frac{1}{8}\left(\frac{hv-\phi}{2\phi}\right)^2\right) + (hv-\phi) \, . \tag{2.18}$$

If an excess energy is much less than the work function, $(hv-\phi) << \phi$, the quantum efficiency (QE) is estimated to be

$$QE(v) \propto (hv-\phi)^2 \tag{2.19}$$

Equation (2.19) shows that the expected QE depends on an excess energy by a quadratic relation.

2.1.2 The Schotty Effect

The electric field component of the radio-frequency (RF) wave, which is used to accelerate electrons inside the resonant cavity, has an influence on the work function of the cathode material. In this section, we consider a reduction of the material's work function due to the electric field component of the RF wave. For this study, we assume that the cathode is made of a perfect conductor. Then, the work function is defined as a total required energy, which is used to separate an electron from its image charge inside a conductor surface. If there is no external electric field, a potential energy of electron and its image charge is related to [19]

$$W_{e\cdot image}(x) = e\Phi_{image}(x) = e\left(\frac{-e}{2x}\right), \tag{2.20}$$

where x is the distance between the electron and the cathode surface. By using the symmetric consideration, the potential energy between the electron and the cathode surface is half of the value in equation (2.20), which is

$$W_{surface}(x) = \left(\frac{-e^2}{4x}\right). \tag{2.21}$$

In classical electromagnetic theory, the work function is defined as the total energy required to move the electron from some minimum distance between the electron and its image charge (x_{min}) to infinity (∞), thus the work function in case of no external electric field becomes

$$\phi_0 = W_{surface}(\infty) - W_{surface}(x_{\min}) = \left(\frac{e^2}{4x_{\min}}\right). \tag{2.22}$$

When an external electric field is applied on the cathode surface, the potential energy of the field is

$$W_{field}(x) = e\Phi_{field}(x) = e(-Ex) = -eEx, \tag{2.23}$$

where E is the magnitude of the electric field, which has the direction perpendicular to the cathode surface. The total potential energy is obtained by

$$W_{total}(x) = W_{surface}(x) + W_{field}(x) = \frac{-e^2}{4x} - eEx. \tag{2.24}$$

A derivative of the total potential energy with respect to the distance is calculated to find the optimal distance (x_0), where the total potential energy reaches a maximum value. The derivative of the total energy is

$$\left.\frac{d}{dx}W_{total}(x)\right|_{x=x_0} = \frac{e^2}{4x_0^2} - eE = 0. \tag{2.25}$$

Then, the maximum total potential energy occurs at $x_0 = (\sqrt{e/E})/2$. Therefore, the maximum total potential energy is

$$W_{total}(x_0) = -e\sqrt{eE}\ . \tag{2.26}$$

When the external electric field is applied, the total work function becomes

$$\phi = W_{total}(x_0) - W_{total}(x_{\min}) = \frac{e^2}{4x_{\min}} - e\sqrt{eE}\ . \tag{2.27}$$

The change in the work function of $-e\sqrt{eE}$ is called the Schottky effect. To convert the result in equation (2.27) to SI unit. The change of the work function due to the Schottky effect is [20]

$$\Delta\phi_{Schottky}[eV] = a\sqrt{E[V/m]}\ , \tag{2.28}$$

where $a = e\sqrt{\dfrac{e}{4\pi\varepsilon_0}} = 3.7947 \times 10^{-5}[e\sqrt{Vm}]$.

The modified work function of the material when the external electric field is applied can be written as

$$\phi = \phi_0 - a\sqrt{E}\ , \tag{2.29}$$

where ϕ_0 is the work function of the material in the absence of the external electric field.

2.2 Acceleration of Electrons in Resonant Cavity

To accelerate electrons inside the photocathode radio-frequency (RF) gun in this study, the RF wave is transported from a high power klystron by a waveguide system and fed into the RF-gun cavity through an aperture hole on the cylindrical wall of the full-cell cavity. Then, the RF wave is coupled to the half-cell cavity via an iris between the two main cavities. The RF wave resonates in both cavities and forms a standing wave pattern, which has the time revolution electric and magnetic field components. The electric field component is used to accelerate the free electrons emitted at the cathode surface via the photoelectric effect to form the electron bunches at the gun exit. For simple explanation, a cylindrical pillbox cavity with the lowest transverse magnetic field mode TM_{010} is discussed here. The shape of the cavity and the field directions inside the TM_{010} pillbox cavity are shown in Fig. 2.1.

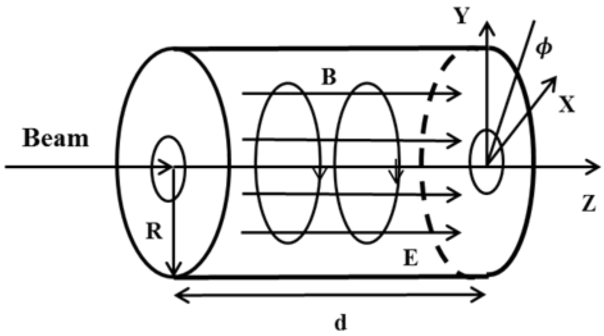

Figure 2.1: TM_{010} pillbox cavity with electric and magnetic field direction.

Wave equations of longitudinal electric field and magnetic field components for free space with no charge and no current are [21]

$$\nabla^2 E_z + k^2 E_z = 0 \quad \text{and} \quad \nabla^2 B_z + k^2 B_z = 0\,, \tag{2.30}$$

where k is the wave number. In cylindrical coordinates (ρ, φ, z), the wave equation of the longitudinal electric field is

$$\frac{1}{r}\frac{\partial}{\partial r}(r\frac{\partial E_z}{\partial r}) + \frac{1}{r^2}\frac{\partial^2 E_z}{\partial \varphi^2} + \frac{\partial^2 E_z}{\partial z^2} + k^2 E_z = 0\,. \tag{2.31}$$

The solution of equation (2.31) can be written is a form of Bessel function $J_m(k_c r)$ as

$$E_z(r, \varphi, z, t) = E_0 J_m(k_c r) e^{\pm im\varphi} e^{\pm ik_z z} e^{i\omega t}\,, \tag{2.32}$$

where ω is the angular frequency of the RF wave. Consider the case of azimuthal symmetry with m = 0 and the boundary condition at the cavity wall of $B_{\parallel} = B_{\perp} = 0$. The electric field component E_z and the magnetic field component B_φ inside the RF pillbox cavity are [21]

$$E_z(r,t) = E_0 J_0(k_c r)\cos\omega t\,, \tag{2.33}$$

$$B_\varphi(r,t) = -\frac{E_0}{c} J_1(k_c r)\sin\omega t\,. \tag{2.34}$$

where $k_c = 2\pi / \lambda_{rf}$ while λ_{rf} is the wavelength of the RF wave and $c = \omega / k_c$. Here, $J_0(k_c r)$ and $J_1(k_c r)$ are the Bessel functions of the zeroth and the first orders as shown in Fig. 2.2.

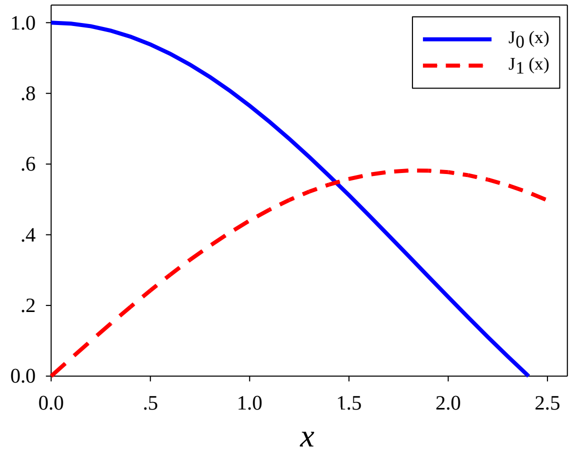

Figure 2.2: Bessel functions of the zero[th] order $J_0(x) = J_0(k_c r)$ and the first order $J_1(x) = J_1(k_c r)$.

According to equation (2.33), the electric field component E_z inside the TM_{010} cavity has the maximum value at $r = 0$ and it decreases when the radial distance in the cavity increases. For the longitudinal direction, the electric field component E_z is constant as shown in Fig. 2.3.

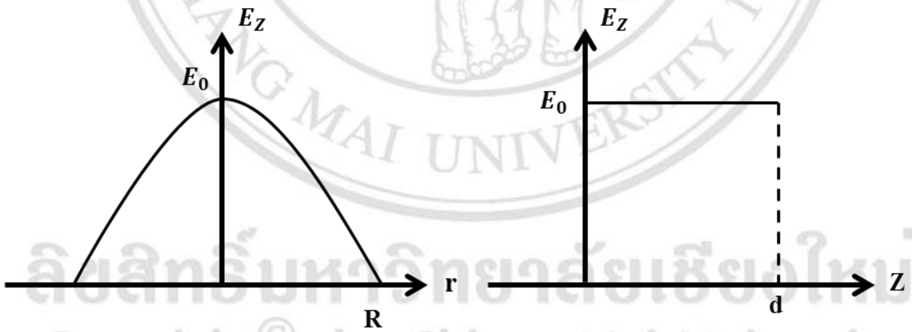

Figure 2.3: Magnitude of the longitudinal electric field E_z as a function of the radius (r) and the longitudinal distance (z) of the TM_{010} pillbox cavity.

The parameters, such as a resonant frequency (f_{rf}), a transit time factor (T_t), a quality factor (Q) and a shunt impedance (R_s), are used to describe the properties of the resonant cavity. Such parameters for the TM_{010} cylindrical pillbox cavity can be evaluated from the cavity geometry and accelerating voltage (V_{acc}). By considering the Bessel function of the zero[th] order in Fig. 2.2, it is found that $J_0(2.405) = 0$ at $k_c r = 2.405$

. Then, we get the relationship between the resonant frequency (f_{rf}) and the cavity radius (R) as

$$f_{rf} = \frac{\omega}{2\pi} = \frac{k_c c}{2\pi\sqrt{\mu\varepsilon}R} = \frac{2.405c}{2\pi R}, \tag{2.35}$$

where μ and ε are the permeability and the permittivity of the medium inside the cavity, respective. In our case the medium is vacuum where $1/\sqrt{\mu\varepsilon} = c$. Then, the RF wavelength is

$$\lambda_{rf} = \frac{c}{f_{rf}} = \frac{2\pi}{2.405}R. \tag{2.36}$$

The radius of the resonant cavity becomes

$$R = 2.405\frac{c}{2\pi f_{rf}} = 2.405\frac{\lambda_{rf}}{2\pi}. \tag{2.37}$$

When an electron is accelerated inside the resonant cavity, the energy gain of the electron can be evaluated from

$$W = eV_{acc} = e\int_{-d/2}^{d/2} E_0 \cos(\omega t)dz, \tag{2.38}$$

where d is the cavity length, v is the electron velocity and $\omega = 2\pi f_{rf}$ is the angular frequency. Thus, the accelerating voltage inside the resonant cavity is

$$V_{acc} = \int_{-d/2}^{d/2} E_0 \cos(\omega z / v)dz = E_0 \frac{2v}{\omega}\sin\frac{\omega d}{2v}. \tag{2.39}$$

A transit time factor (T_t), which is defined by a ratio of the energy gain from the acceleration in one RF period and the maximum energy gain, is

$$T_t = \frac{V_{acc}}{E_0 d} = \frac{\sin(\omega d / 2v)}{\omega d / 2v}. \tag{2.40}$$

From the synchronism condition of the π-mode acceleration, the length of cavity is

$$d = \frac{vT_{rf}}{2} = \beta\frac{\lambda_{rf}}{2}, \tag{2.41}$$

where T_{rf} is the RF period and $\beta = v/c$. To get a maximum energy gain, the electron must be accelerated at the RF phase of $\pi/2$. Therefore, the transit time factor for the maximum acceleration case is

$$T_t = \frac{\sin(\pi/2)}{\omega d/2v} = \frac{2v}{\omega d} = \frac{2(\lambda_{rf} f_{rf})}{(2\pi f_{rf})(\beta\lambda_{rf}/2)} = \frac{2}{\pi}. \tag{2.42}$$

For the relativistic electron with the velocity close to the velocity of light ($\beta \approx 1$), the maximum accelerating voltage for the π-mode RF structure is

$$V_{acc} = E_0 d T_t = \frac{2E_0 d}{\pi}. \tag{2.43}$$

A quality factor (Q-factor) describes a relationship between the stored energy inside the cavity (W_s) and the dissipated power that dissipates into the cavity wall (P_{cy}) in one RF period. It is normally used to define the acceleration efficiency inside the RF cavity, which is written as

$$Q = \frac{\omega W_s}{P_{cy}}. \tag{2.44}$$

It can be seen from equation (2.44) that the resonant cavity with large Q-factor value can store a large amount of energy for charged particle acceleration inside the cavity. The stored energy inside the resonant cavity and the power dissipated into the cavity wall in term of the magnetic field are

$$W_s = \frac{1}{2\mu_0}\int B^2 dV, \tag{2.45}$$

$$P_{cy} = \frac{R_w}{2\mu_0^2}\int B^2 da, \tag{2.46}$$

where μ_0 is the permeability of vacuum and $R_w = \rho_c/\delta$ is the surface resistance of the cavity wall, while ρ_c and δ are the resistivity and the skin depth of the cavity material, respectively. The skin depth of the cavity material can be calculated from

$$\delta = \sqrt{\frac{2\rho_c}{\mu_0\omega}} = \sqrt{\frac{2}{\mu_0\omega\sigma_c}}, \tag{2.47}$$

where $\sigma_c = 1/\rho_c$ is the conductivity of the cavity material. Then, we can evaluate the Q-factor of the cavity from

$$Q = \frac{\omega W_s}{P_{cy}} = \frac{2\int B^2 dV}{\delta \int B^2 ds} .$$

Due to the resistance property of the resonant cavity, the power loss into the cavity wall is

$$P_{cy} = \frac{V_{acc}^2}{R_s} , \tag{2.48}$$

where R_s is the shunt impedance of the cavity. Thus, the shunt impedance per unit length (r_s) is

$$r_s = \frac{V_{acc}^2}{P_{cy} d} = \frac{E_0^2 d}{P_{cy}} T_t^2 . \tag{2.49}$$

Then, the cavity wall loss power (P_{cy}) can be obtained from

$$P_{cy} = \frac{V_{acc}^2}{r_s d} = \frac{E_0^2 d}{r_s} , \tag{2.50}$$

where E_0 is the accelerating gradient of the longitudinal electric field and d is the effective length of the cavity. If the RF-gun has more than one resonant cavities, the cavity wall loss of the n cavities becomes

$$P_{cy} = \frac{E_1^2 d_1}{r_{s1}} + \frac{E_2^2 d_2}{r_{s2}} + ... + \frac{E_n^2 d_n}{r_{sn}} . \tag{2.51}$$

The amplitude of the longitudinal electric field component $E_z(z,t)$ of the RF wave as a function of the revolution time and the longitudinal z-coordinate can be written as

$$E_z(z,t) = E_0(z) \sin(\omega t + \varphi) , \tag{2.52}$$

where $E_0(z)$ is the amplitude of the electric field, $\omega = 2\pi f_{rf}$ is the angular resonant frequency, t is the RF revolution time and φ is the initial RF phase difference. The energy gain (ΔW) of the electron, which is accelerated through the resonant cavity is calculated to be

$$\Delta W = W_0 + \int_0^{T_{rf}/2} eE_0(z) \cdot \sin(\omega t + \varphi) dt , \tag{2.53}$$

where W_0 is initial electron energy before it enters the cavity, T_{rf} is the RF period and $z = ct$. Then, the energy gain of the electron becomes

$$\Delta W = W_0 + \int_0^{T_{rf}/2} e\cos(\varphi) E_0(ct)\sin(\omega t)dt + \int_0^{T_{rf}/2} e\sin(\varphi) E_0(ct)\cos(\omega t)dt . \quad (2.54)$$

The second integration in equation (2.54) equals to zero because it integrates an odd function in half period. Thus, the energy gain of the electron when it exits from the resonant cavity is

$$\Delta W = W_0 + eV_{acc}\cos(\varphi) , \quad (2.55)$$

where $V_{acc} = \int_0^{T_{rf}/2} E(ct)\sin(\omega t)dt$ is the accelerating voltage in the cavity. Equation (2.55) is modified when the electron enters the resonant cavity at any phase φ. This results in the energy gain of

$$\Delta W = W_0 + eV_{acc}\cos(\varphi - \varphi_0) . \quad (2.56)$$

Here φ_0 is the phase that the electron achieves the maximum possible energy gain or the so called maximum mean momentum gain (MMMG) phase. A model of the electron bunch acceleration by the RF wave is shown in Fig. 2.4, which the RF phase increases from left to right. The blue line refers to the electron momentum gain p_z, which is a function of the RF phase. The head of electron bunch enters first to the resonant cavity and experiences an earlier phase than the tail of the bunch. If the entire bunch enters the cavity earlier than the MMMG phase (φ_0) with a phase difference of $\Delta\varphi = \varphi - \varphi_0$, the tail of the bunch will achieve higher acceleration than the head.

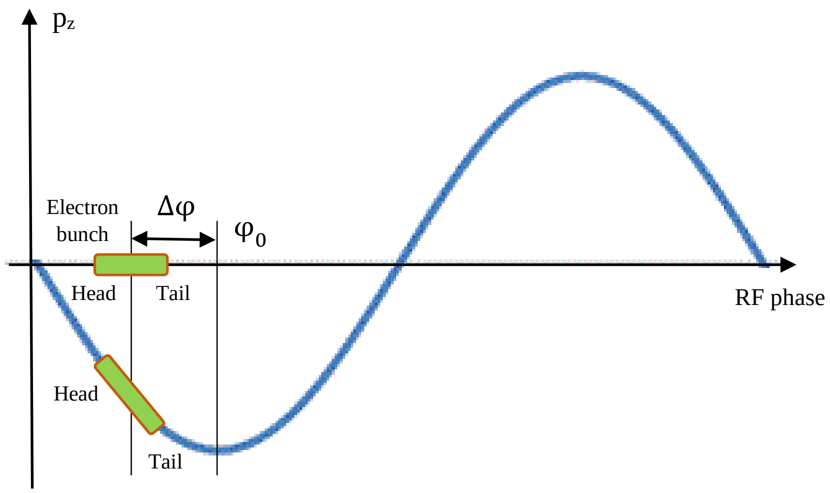

Figure 2.4: Model of the electron bunch acceleration inside the resonant cavity [22].

2.3 Bending and Focusing of Electron Beam

When an electron travels through a transverse magnetic field, which is perpendicular to the electron's direction, there is a magnetic force acts on the electron and changes its traveling direction. Generally, dipole and quadrupole magnetic fields are used to bend the electron beam trajectory and to control the beam transverse size, respectively. In practice, the dipole and quadrupole magnets do not have only dipole or quadrupole fields. They may have multipole-field components. This is due to the magnet construction limitation. By considering the multipole-field expansion using the Taylor's expansion, the transverse magnetic field is

$$\vec{B} = B_x \hat{x} + B_y \hat{y} \,. \tag{2.57}$$

The transverse magnetic field B_x and B_y can be expanded around the point $x = 0$ and $y = 0$ as

$$B_x = B_{x0} + \left(\frac{\partial B_x}{\partial x}\right)\bigg|_{x=0} x + \left(\frac{\partial B_x}{\partial y}\right)\bigg|_{x=0} y + \frac{1}{2}\left(\frac{\partial^2 B_x}{\partial x^2}\right)\bigg|_{x=0} x^2 + \left(\frac{\partial^2 B_x}{\partial x \partial y}\right)\bigg|_{x=0} xy + \frac{1}{2}\left(\frac{\partial^2 B_x}{\partial y^2}\right)\bigg|_{x=0} y^2 + \ldots$$

$$B_y = B_{y0} + \left(\frac{\partial B_y}{\partial x}\right)\bigg|_{y=0} x + \left(\frac{\partial B_y}{\partial y}\right)\bigg|_{y=0} y + \frac{1}{2}\left(\frac{\partial^2 B_y}{\partial x^2}\right)\bigg|_{y=0} x^2 + \left(\frac{\partial^2 B_y}{\partial x \partial y}\right)\bigg|_{y=0} xy + \frac{1}{2}\left(\frac{\partial^2 B_y}{\partial y^2}\right)\bigg|_{y=0} y^2 + \ldots$$

where B_{x0} and B_{y0} are the uniform magnetic fields in the x-axis and the y-axis, respectively. In the region where is no charge and no electric current, the curl and the divergence of the magnetic field are

$$\vec{\nabla} \times \vec{B} = 0 \qquad \text{and} \qquad \vec{\nabla} \cdot \vec{B} = 0 . \tag{2.58}$$

The curl of the magnetic field can be written as

$$\vec{\nabla} \times \vec{B} = \begin{vmatrix} \hat{x} & \hat{y} & \hat{z} \\ \frac{\partial}{\partial x} & \frac{\partial}{\partial y} & \frac{\partial}{\partial z} \\ B_x & B_y & 0 \end{vmatrix} = \left(\frac{\partial B_y}{\partial x} - \frac{\partial B_x}{\partial y} \right) \hat{z} = 0 .$$

Then, we get $\quad \dfrac{\partial B_y}{\partial x} = \dfrac{\partial B_x}{\partial y} \quad$ and $\quad \dfrac{\partial^2 B_y}{\partial x^2} = \dfrac{\partial B_x}{\partial x \partial y} = -\dfrac{\partial^2 By}{\partial y^2}$.

The divergence of the magnetic field is

$$\vec{\nabla} \cdot \vec{B} = \left(\frac{\partial}{\partial x} \hat{x} + \frac{\partial}{\partial y} \hat{y} + \frac{\partial}{\partial z} \hat{z} \right) \cdot \left(B_x \hat{x} + B_y \hat{y} \right) = \frac{\partial B_x}{\partial x} + \frac{\partial B_y}{\partial y} = 0$$

Thus, the magnetic gradients and the derivatives of the magnetic gradient are

$$\frac{\partial B_x}{\partial x} = -\frac{\partial B_y}{\partial y} \qquad \text{and} \qquad \frac{\partial^2 B_x}{\partial x^2} = -\frac{\partial B_y}{\partial x \partial y} = -\frac{\partial^2 B_x}{\partial y^2} .$$

Then, the multipole-field expansions in the x-axis and the y-axis become

$$B_x(x,y) = B_{y0} + \frac{\partial B_x}{\partial x} x - \frac{\partial B_x}{\partial y} y + \frac{1}{2} \frac{\partial^2 B_x}{\partial x^2} (x^2 - y^2) + \frac{\partial^2 B_x}{\partial x \partial y} xy + \ldots , \tag{2.59}$$

$$B_y(x,y) = B_{x0} + \frac{\partial B_y}{\partial x} x - \frac{\partial B_y}{\partial y} y + \frac{1}{2} \frac{\partial^2 B_y}{\partial x^2} (x^2 - y^2) + \frac{\partial^2 B_y}{\partial x \partial y} xy + \ldots \tag{2.60}$$

where the zeroth, the first and the second order terms are the dipole, quadrupole and sextupole magnetic field components, respectively.

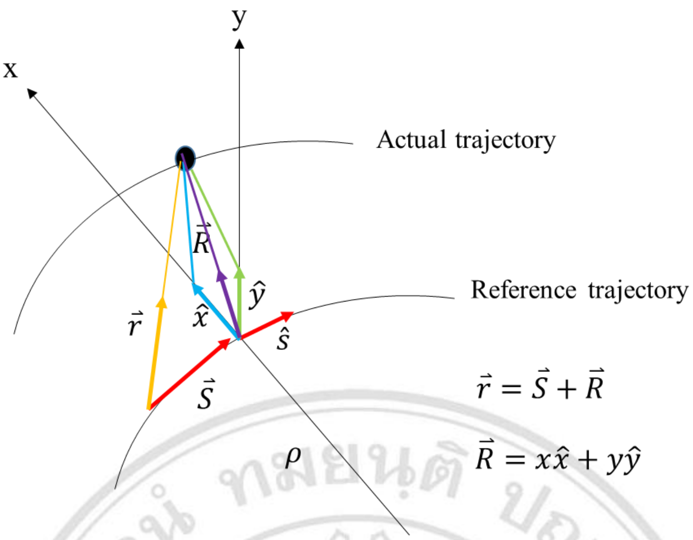

Figure 2.5: Reference and actual trajectories of the electron [23].

In any particle accelerator, a reference trajectory is a design path of the reference particle in the accelerator. As shown in Fig. 2.5, the reference trajectory is defined in the curvilinear coordinates with the unit vectors $(\hat{x}, \hat{y}, \hat{s})$ and a displacement vector of the particle is given by

$$\vec{r} = s\hat{s} + x\hat{x} + y\hat{y} . \tag{2.61}$$

According to Newton's second law, the equation of motion of a relativistic particle is related to

$$\vec{F} = \gamma m_0 \ddot{\vec{r}} . \tag{2.62}$$

Since the unit vector $\hat{s}$ is parallel to the reference trajectory and an angular displacement in the y-axis is kept to be constant, thus $\dot{\hat{s}} = 0$ and $\dot{\hat{y}} = 0$ in this consideration. Therefore, the velocity of the electron becomes

$$\dot{\vec{r}} = \left(s\dot{\hat{s}} + \dot{s}\hat{s}\right) + \left(x\dot{\hat{x}} + \dot{x}\hat{x}\right) + \left(y\dot{\hat{y}} + \dot{y}\hat{y}\right) = \dot{s}\hat{s} + x\dot{\hat{x}} + \dot{x}\hat{x} + \dot{y}\hat{y} \tag{2.63}$$

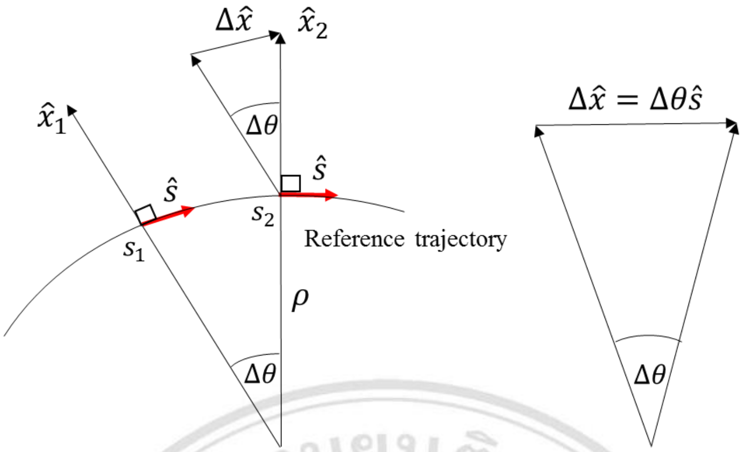

Figure 2.6: Change of the horizontal and vertical displacements with respect to time in s direction [23].

A derivative of the displacement with respect to time is shown in Fig. 2.6. Then, we get $\dot{\hat{x}} = \theta\dot{\hat{s}}$ and $\dot{s} = \rho\dot{\theta}$, where ρ is the curvature radius of the bending trajectory. Thus, the velocity of the electron is

$$\dot{\vec{r}} = (\rho + x)\dot{\theta}\hat{s} + \dot{x}\hat{x} + \dot{y}\hat{y} = \left(1 + \frac{x}{\rho}\right)\dot{s}\hat{s} + \dot{x}\hat{x} + \dot{y}\hat{y} \tag{2.64}$$

By using the relation $\Delta\hat{s} = -\Delta\theta\hat{x}$ or $\dot{\hat{s}} = -\dot{\theta}\hat{x}$, the electron acceleration can be expressed as

$$\ddot{\vec{r}} = \left[\ddot{x} - \left(1 + \frac{x}{\rho}\right)\frac{\dot{s}^2}{\rho}\right]\hat{x} + \ddot{y}\hat{y} + \left(\frac{2\dot{x}\dot{s}}{\rho}\right)\hat{s}\,. \tag{2.65}$$

Apply the Lorentz force to the charge q, $\vec{F} = q\left(\vec{v} \times \vec{B}\right)$, and the equation of motion, $\vec{F} = \gamma m_0\ddot{\vec{r}}$, to equation (2.65), we get

$$\ddot{\vec{r}} = \left[\ddot{x} - \left(1 + \frac{x}{\rho}\right)\frac{\dot{s}^2}{\rho}\right]\hat{x} + \ddot{y}\hat{y} + \left(\frac{2\dot{x}\dot{s}}{\rho}\right)\hat{s} = \left(\frac{q}{\gamma m_0}\right)\left(\vec{v} \times \vec{B}\right),$$

$$\ddot{\vec{r}} = \left[\ddot{x} - \left(1 + \frac{x}{\rho}\right)\frac{\dot{s}^2}{\rho}\right]\hat{x} + \ddot{y}\hat{y} + \left(\frac{2\dot{x}\dot{s}}{\rho}\right)\hat{s} = \left(\frac{q}{\gamma m_0}\right)\left[-v_s B_y\hat{x} + v_s B_x\hat{y} + \left(v_x B_y - v_y B_x\right)\hat{s}\right],$$

where $\vec{v} = v_x\hat{x} + v_y\hat{y} + v_s\hat{s}$ and $\vec{B} = B_x\hat{x} + B_y\hat{y}$. When the electron travelling thought the transverse magnetic field, the transverse accelerations in the x-axis and the y-axis are

$$\ddot{x} - \left(1 + \frac{x}{\rho}\right)\frac{\dot{s}^2}{\rho} = -\left(\frac{q}{\gamma m_0}\right)v_s B_y \qquad \text{and} \qquad \ddot{y} = \left(\frac{q}{\gamma m_0}\right)v_s B_x ,$$

By replacing $v_s = \left(1 + (x/\rho)\right)\dot{s}$, we get

$$\ddot{x} - \left(1 + \frac{x}{\rho}\right)\frac{\dot{s}^2}{\rho} = -\frac{qB_y}{\gamma m_0}\left(1 + \frac{x}{\rho}\right)\dot{s} \qquad \text{and} \qquad \ddot{y} = \frac{qB_x}{\gamma m_0}\left(1 + \frac{x}{\rho}\right)\dot{s} .$$

By using the chain rule, which are $\dot{x} = x'\dot{s}$, $\ddot{x} = \dot{s}^2 x''$, $\dot{y} = y'\dot{s}$ and $\ddot{y} = \dot{s}^2 y''$, the derivatives with respect to time are changed to be the derivatives with respect to the longitudinal distance (s) as

$$x'' - \frac{1}{p}\left(1 + \frac{x}{\rho}\right) = -\frac{qB_y}{\gamma m_0 \dot{s}}\left(1 + \frac{x}{\rho}\right) \qquad \text{and} \qquad y'' = \frac{qB_x}{\gamma m_0 \dot{s}}\left(1 + \frac{x}{\rho}\right).$$

Practically, we need to control the beam to travel close to the reference trajectory as much as possible. That means the transverse displacements are very small. Thus, it can be estimated that $\dot{x} = v_x \to 0$, $\dot{y} = v_y \to 0$, $v_s \approx v$ and $\dot{s} \approx v/(1 + (x/\rho))$. By replacing $\gamma m_0 v$ with a momentum p, the equations of motion of charge q through the transverse magnetic field, which bends the particle trajectory in x-axis, are

$$x'' - \frac{1}{\rho}\left(1 + \frac{x}{\rho}\right) = -\frac{qB_y}{p}\left(1 + \frac{x}{\rho}\right)^2 \qquad \text{and} \qquad y'' = \frac{qB_x}{p}\left(1 + \frac{x}{\rho}\right)^2. \qquad (2.66)$$

On the other hand, the equations of motion of the positive charged particle through the transverse magnetic field, which bends the particle trajectory in the y-axis, are

$$x'' = \frac{qB_y}{p}\left(1 + \frac{y}{\rho}\right)^2 \qquad \text{and} \qquad y'' - \frac{1}{\rho}\left(1 + \frac{y}{\rho}\right) = -\frac{qB_x}{p}\left(1 + \frac{y}{\rho}\right)^2. \qquad (2.67)$$

As mentioned earlier that in this study we focus on the use of the transverse magnetic fields from the dipole and the quadrupole magnets. Therefore, the principles and equation of motions for both magnets are discussed in the following sections. In addition, the principle concerning a solenoid magnet, which has a longitudinal magnetic field, is also discussed.

2.3.1 Dipole Magnet

Consider a simple dipole magnet with a cross section diagram shown in Fig. 2.7. The magnet consists of two magnetic poles, which their pole faces are parallel to each other. Each pole has a coil of n turns with an applied current I. A gap between the two poles is given by G and the magnetic field H_0 in the gap is considered to be uniform. As shown in Fig. 2.7, an induced magnetic field inside the dipole magnetic poles and in the gap can be studied by using Ampere's law as shown in the following equation

$$\oint_c \vec{H} \cdot d\vec{l} = I_{enclosed} = nI \ . \tag{2.68}$$

By considering entire region of the dipole magnet, equation (2.68) becomes

$$\oint_c \vec{H} \cdot d\vec{l} = \int_0^h \vec{H}_0 \cdot d\vec{l} + \int_0^{l_{Fe}} \vec{H}_{Fe} \cdot d\vec{l} = H_0 G + H_{Fe} l_{Fe} = nI \ .$$

For an iron yoke and poles with a large permeability of $\mu_r >> 1$, the magnetic field inside the yoke and the poles is nearly zero, $\vec{H} = (\vec{B}/\mu_r) \to 0$. Then, equation (2.68) becomes

$$\oint_c \vec{H} \cdot d\vec{l} = H_0 G + 0 = nI \ .$$

Thus, the magnetic field in the gap between the poles is

$$B_0 = \frac{\mu_0 nI}{G}, \tag{2.69}$$

where μ_0 is the permeability of free space, which is equal to $4\pi \times 10^{-7}$ [kg m s^{-2} A^{-2}].

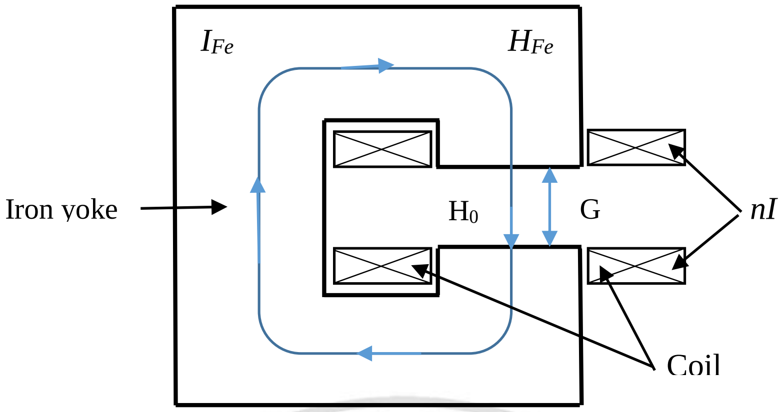

Figure 2.7: Cross section diagram of a simple dipole magnet [24].

When the charged particle beam travels through the uniform transverse magnetic field, the equation of motion of a moving particle with charge *g* is

$$F = \frac{\gamma m_0 v^2}{\rho} = qvB_0 \,. \tag{2.70}$$

A traveling path of the beam is bent with a curvature radius ρ as defined in this following equation

$$\frac{1}{\rho} = \frac{\theta}{l} = \frac{qB_0}{p}, \tag{2.71}$$

where B_0 is the uniform transverse magnetic field, θ is the bending angle, l is the path length of the charged particle beam in the magnetic field, q is the charge of particle and p is the particle momentum. In case of electron with charge e, the relationship between the curvature radius, the magnetic field and the electron energy becomes [25]

$$\frac{1}{\rho[m]} = \frac{eB_0}{p} = \frac{0.2998 B_0[T]}{p[GeV/c]} \,. \tag{2.72}$$

Equation (2.72) shows that electrons with different energies bend in the uniform dipole magnetic field with different bending radii.

In case of the dipole magnetic field, which $B_y = B_{y0} = B_0$ and $B_x = 0$, the electron bends in the x-axis with the following equations of motion

$$x'' - \frac{1}{\rho}\left(1+\frac{x}{\rho}\right) = -\frac{qB_0}{p}\left(1+\frac{x}{\rho}\right)^2 \qquad \text{and} \qquad y'' = 0 \ .$$

When a beam rigidity is defined as $B_0\rho \equiv \frac{\gamma m_0 v}{q} = \frac{p}{q}$, we get

$$x'' - \frac{1}{\rho}\left(1+\frac{x}{\rho}\right) = -\frac{1}{\rho}\left(1+\frac{x}{\rho}\right)^2 . \tag{2.73}$$

If the displacement in the x-axis is small, the terms x^2, xy, y^2,… are very small and can be neglected. The equations of motion become

$$x'' - \frac{1}{\rho} - \frac{x}{\rho^2} = -\frac{1}{\rho}\left(1+\frac{2x}{\rho}+\frac{x^2}{\rho^2}\right)$$

or
$$x'' + \frac{x}{\rho^2} = 0 \tag{2.74}$$

Equation (2.74) is in the form of the Hill's equation, which has the solutions in the forms of

$$x = C_1\cos(\frac{s}{\rho}) + C_2\sin(\frac{s}{\rho}) \quad \text{and} \quad x'' = -\frac{C_1}{\rho}\sin(\frac{s}{\rho}) + \frac{C_2}{\rho}\cos(\frac{s}{\rho}) \ .$$

By using the initial conditions of $s = 0$, $x = x_0$ and $x' = x_0'$, the coefficients $C_1 = x_0$ and $C_2 = \rho x_0'$ are achieved. Thus, the solutions of the equations of motion are

$$x = \cos(\frac{s}{\rho})x_0 + \rho\sin(\frac{s}{\rho})x_0' \quad \text{and} \quad x'' = -\frac{1}{\rho}\sin(\frac{s}{\rho})x_0 + \cos(\frac{s}{\rho})x_0' \ .$$

The above equations can be written in a form of the beam transport matrix M_x as

$$\begin{bmatrix} x \\ x' \end{bmatrix} = \begin{bmatrix} \cos(\frac{s}{\rho}) & \rho\sin(\frac{s}{\rho}) \\ -\frac{1}{\rho}\sin(\frac{s}{\rho}) & \cos(\frac{s}{\rho}) \end{bmatrix} \begin{bmatrix} x_0 \\ x_0' \end{bmatrix} = M_x \begin{bmatrix} x_0 \\ x_0' \end{bmatrix}, \tag{2.75}$$

where s and ρ are the arc length and the bending radius, respectively. For non-deflecting plane, $y'' = 0$, the solutions of the equations of motion are

$$y = C_1' + C_2' s \qquad \text{and} \qquad y' = C_2' .$$

By using the initial conditions of $s = 0$, $y = y_0$ and $y' = y_0'$, the coefficients $C_1' = y_0$ and $C_2' = y_0'$ are achieved. The solutions of the equations of motion can be written in the form of the matrix transportation as

$$\begin{bmatrix} y \\ y' \end{bmatrix} = \begin{bmatrix} 1 & s \\ 0 & 1 \end{bmatrix} \begin{bmatrix} y_0 \\ y_0' \end{bmatrix}. \tag{2.76}$$

Thus, the transport matrix for the non-deflecting plane of the dipole magnet is

$$M_y = \begin{bmatrix} 1 & s \\ 0 & 1 \end{bmatrix}. \tag{2.77}$$

By including both transverse directions, the 4-dimensional matrix transportation of the dipole magnet, which bends the positive charged particle in the x-axis is written by

$$\begin{bmatrix} x \\ x' \\ y \\ y' \end{bmatrix} = \begin{bmatrix} \cos(\frac{s}{\rho}) & \rho \sin(\frac{s}{\rho}) & 0 & 0 \\ -\frac{1}{\rho}\sin(\frac{s}{\rho}) & \cos(\frac{s}{\rho}) & 0 & 0 \\ 0 & 0 & 1 & s \\ 0 & 0 & 0 & 1 \end{bmatrix} \begin{bmatrix} x_0 \\ x_0' \\ y_0 \\ y_0' \end{bmatrix}. \tag{2.78}$$

Similarly, the 4-dimensional matrix transportation of the dipole magnet, which bends the positive charged particle in the y-axis is

$$\begin{bmatrix} x \\ x' \\ y \\ y' \end{bmatrix} = \begin{bmatrix} 1 & s & 0 & 0 \\ 0 & 1 & 0 & 0 \\ 0 & 0 & \cos(\frac{s}{\rho}) & \rho \sin(\frac{s}{\rho}) \\ 0 & 0 & -\frac{1}{\rho}\sin(\frac{s}{\rho}) & \cos(\frac{s}{\rho}) \end{bmatrix} \begin{bmatrix} x_0 \\ x_0' \\ y_0 \\ y_0' \end{bmatrix}. \tag{2.79}$$

2.3.2 Quadrupole Magnet

Generally, a quadrupole magnet is used to focus or defocus the charged particle beam. A cross sectional diagram of the quadrupole magnet (as shown in Fig. 2.8) consists of four magnetic poles, which each pole has a coil of N turns and an applied current I. A radius of an aperture between the four poles is given by R.

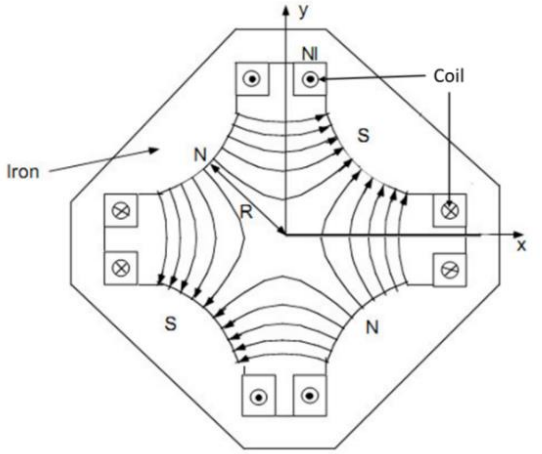

Figure. 2.8: Cross section diagram of a quadrupole magnet [25].

The magnetic field inside the aperture between the four poles increases linearly when the distance from the center of the magnet increases. Thus, the quadrupole magnet has constant magnetic field gradients, which are $\frac{\partial B_x}{\partial y} \neq 0$, $\frac{\partial B_y}{\partial y} = 0$, $\frac{\partial B_y}{\partial x} \neq 0$ and $\frac{\partial B_x}{\partial x} = 0$. From these conditions, the induced magnetic fields in the vertical and horizontal directions are written in the terms of magnetic field gradients g_x and g_y as

$$B_x(x, y) = (\frac{\partial B_x}{\partial y})y = g_x y, \tag{2.80}$$

$$B_y(x, y) = (\frac{\partial B_y}{\partial x})x = g_y x. \tag{2.81}$$

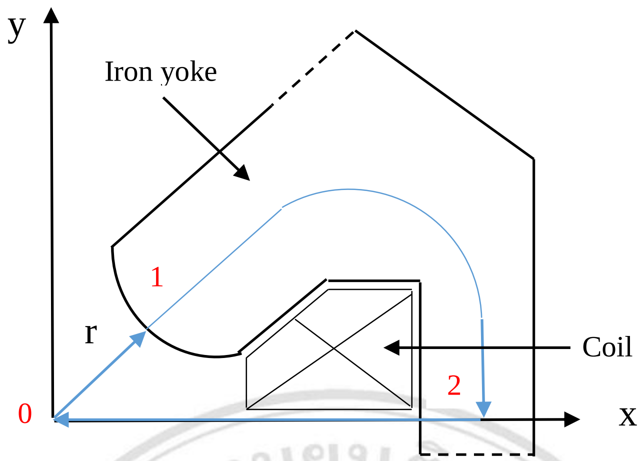

Figure 2.9: Cross sectional diagram of a single pole of the quadrupole magnet.

An induced magnetic field of the dipole magnet can be derived by using the Ampere's law. According to the integration path in Fig. 2.9, we get

$$\oint_c \vec{H}\cdot d\vec{l} = I_{enclosed} = NI\ , \tag{2.82}$$

$$\oint_c \vec{H}\cdot d\vec{l} = \int_0^1 \vec{H}\cdot d\vec{r} + \int_1^2 \vec{H}_{Fe}\cdot d\vec{l} + \int_2^0 \vec{H}\cdot d\vec{l}\ . \tag{2.83}$$

Consider an iron yoke and pole with large permeability of $\mu_r >> 1$, the magnetic field inside the yoke and pole whose the path from point 1 to point 2, is nearly zero or $\vec{H}_{Fe} = (\vec{B}_{Fe}/\mu_r) \rightarrow 0$. The path from point 2 to point 0 gives $\vec{H}\cdot d\vec{l} = 0$ because the direction of the magnetic field $\vec{B}$ is perpendicular to the direction of $d\vec{l}$. As the total transverse magnetic field amplitude is obtained from $B = \sqrt{B_x^2 + B_y^2}$, thus the magnetic field H in the gap is

$$H = \frac{B(x,y)}{\mu_0} = \frac{1}{\mu_0}\sqrt{B_x^2 + B_y^2} = \frac{g}{\mu_0}\sqrt{x^2 + y^2} = \frac{g}{\mu_0} r\ . \tag{2.84}$$

where g is the gradient of the magnetic field and in this case we consider that $g_x = g_y = g$. By using equation (2.84), equation (2.83) becomes

$$\oint_c \vec{H}\cdot d\vec{l} = \frac{1}{\mu_0}\int_0^r grdr = \frac{gr^2}{2\mu_0} = NI\ . \tag{2.85}$$

Therefore, the gradient of the quadrupole magnet is

$$g = B' = \frac{2\mu_0 NI}{r^2}, \tag{2.86}$$

Consider equations of motion of a moving charged particle inside the quadrupole magnetic field as

$$x'' = -\frac{qB_y}{p}(1+\frac{x}{p})^2 \quad \text{and} \quad y'' = \frac{qB_x}{p}(1+\frac{y}{\rho})^2 .$$

When a strength of the quadrupole magnet is given by

$$k = k_x^2 = -k_y^2 = \frac{qg}{p}, \tag{2.87}$$

Thus, the equation of motion in horizontal axis becomes

$$x'' + \frac{qg}{p}x = 0 . \tag{2.88}$$

In case of $k_x^2 = (qg/p) > 0$, equation (2.88) becomes $x'' + kx = 0$, which has the solutions in the form of

$$x = C_1\cos(\sqrt{k}s) + C_2\sin(\sqrt{k}s) \quad \text{and} \quad x' = -\sqrt{k}\sin(\sqrt{k}s) + \sqrt{k}\cos(\sqrt{k}s) .$$

By using the initial conditions of $s = 0$, $x = x_0$ and $x' = x_0'$, the coefficients $C_1 = x_0$ and $C_2 = (1/\sqrt{k})x_0'$ are achieved. Thus, the solutions of equations of motion in horizontal axis of the quadrupole magnet with an effective length l are

$$x = \cos(\sqrt{k}l)x_0 + (1/\sqrt{k})\sin(\sqrt{k}l)x_0' \quad \text{and} \quad x' = -\sqrt{k}\sin(\sqrt{k}l)x_0 + \cos(\sqrt{k}l)x_0' .$$

The solutions in the x-axis can be written in the form of the matrix transportation as

$$\begin{bmatrix} x \\ x' \end{bmatrix} = \begin{bmatrix} \cos(\sqrt{k}l) & (1/\sqrt{k})\sin(\sqrt{k}l) \\ -\sqrt{k}\sin(\sqrt{k}l) & \cos(\sqrt{k}l) \end{bmatrix} \begin{bmatrix} x_0 \\ x_0' \end{bmatrix} . \tag{2.89}$$

In the y-axis, the equation of motion is

$$y'' - \frac{qg}{p} = 0 \ . \tag{2.90}$$

Similar to the case of the x-axis, the solution in the y-axis can be written in the form of the matrix transportation as

$$\begin{bmatrix} y \\ y' \end{bmatrix} = \begin{bmatrix} \cosh(\sqrt{|k|}l) & (1/\sqrt{|k|})\sinh(\sqrt{|k|}l) \\ \sqrt{|k|}\sinh(\sqrt{|k|}l) & \cosh(\sqrt{|k|}l) \end{bmatrix} \begin{bmatrix} y_0 \\ y_0' \end{bmatrix}. \tag{2.91}$$

Therefore, the 4-dimensional matrix transportation of the focusing quadrupole magnet is

$$\begin{bmatrix} x \\ x' \\ y \\ y' \end{bmatrix} = \begin{bmatrix} \cos(\sqrt{k}l) & (1/\sqrt{k})\sin(\sqrt{k}l) & 0 & 0 \\ -\sqrt{k}\sin(\sqrt{k}l) & \cos(\sqrt{k}l) & 0 & 0 \\ 0 & 0 & \cosh(\sqrt{|k|}l) & (1/\sqrt{|k|})\sinh(\sqrt{|k|}l) \\ 0 & 0 & \sqrt{|k|}\sinh(\sqrt{|k|}l) & \cosh(\sqrt{|k|}l) \end{bmatrix} \begin{bmatrix} x_0 \\ x_0' \\ y_0 \\ y_0' \end{bmatrix}. \tag{2.92}$$

Similarly, the 4-dimensional matrix transportation of the defocusing quadrupole magnet is

$$\begin{bmatrix} x \\ x' \\ y \\ y' \end{bmatrix} = \begin{bmatrix} \cosh(\sqrt{|k|}l) & (1/\sqrt{|k|})\sinh(\sqrt{|k|}l) & 0 & 0 \\ \sqrt{|k|}\sinh(\sqrt{|k|}l) & \cosh(\sqrt{|k|}l) & 0 & 0 \\ 0 & 0 & \cos(\sqrt{k}l) & (1/\sqrt{k})\sin(\sqrt{k}l) \\ 0 & 0 & -\sqrt{k}\sin(\sqrt{k}l) & \cos(\sqrt{k}l) \end{bmatrix} \begin{bmatrix} x_0 \\ x_0' \\ y_0 \\ y_0' \end{bmatrix}. \tag{2.93}$$

When the electron beam travels through the quadrupole magnet, the effective length is evaluated by

$$l = \frac{\int g\,dz}{\langle g \rangle}, \tag{2.94}$$

where $<g>$ is the average of the magnetic gradient near the center of the magnet. The quadrupole magnetic field can be used to focus the electron beams with a focal length of

$$f[m] = \frac{1}{k[m^{-2}]l[m]}. \tag{2.95}$$

Therefore, the strength of the quadrupole magnet becomes [25

$$k[m^{-2}] = \frac{0.2998G[T/m]}{p[Gev/c]} \tag{2.96}$$

2.3.3 Solenoid Magnet

Properties of a solenoid magnet are equivalent to optical lens, which can be used to focus the charged particle beam in both x-axis and y-axis. A diagram of the solenoid magnet and an induced magnetic field lines are shown in Fig. 2.10. A relationship between the induced magnetic field $\vec{H}$ and an applied current I is obtained by using the Ampere's law as

$$\oint_c \vec{H} \cdot d\vec{l} = I_{encloed} = NI \,,$$

$$\oint_c \vec{H} \cdot d\vec{l} = \int_0^l \frac{B_z}{\mu_0} dl = \frac{B_z l}{\mu_0} = NI \,,$$

where l is the physical length of the solenoid magnet and N is the number of coil's turns. Thus, a longitudinal magnetic field component (B_z) inside the solenoid, which is parallel to the traveling direction of the beam, is calculated to be

$$B_z = \frac{\mu_0 NI}{l} \,. \tag{2.97}$$

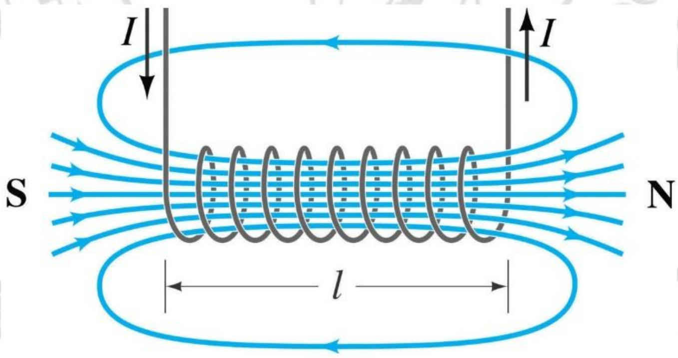

Figure 2.10: Diagram of the solenoid magnet and the induced magnetic field lines [26].

Inside the ideal solenoid magnet, the magnetic field B_z is constant and there is no transverse magnetic field components B_x and B_y. However, there is a coupling condition between B_x and B_y at the entrance and the exit edges of the solenoid magnet. Therefore, the solenoid magnet focuses the beam in both x-axis and y-axis with the edge fields of [27]

$$B_x = -\frac{1}{2}\frac{\partial B_z}{\partial z} x \qquad \text{and} \qquad B_y = -\frac{1}{2}\frac{\partial B_z}{\partial z} y \,. \tag{2.98}$$

Equation (2.98) shows that the solenoid magnet has the magnetic field gradients at the longitudinal edges similar to the quadrupole magnetic fields. The beam matrix at the entrance edge of the solenoid magnet is [27]

$$M_1 = \begin{bmatrix} 1 & 0 & 0 & 0 \\ 0 & 1 & \frac{eB_z}{2p} & 0 \\ 0 & 0 & 1 & 0 \\ -\frac{eB_z}{2p} & 0 & 0 & 1 \end{bmatrix}, \tag{2.99}$$

where B_z is the magnetic field along the z-axis, p_z is the particle momentum component in the z-axis with the approximation $p_z \approx p$, while $p = \sqrt{p_x^2 + p_y^2 + p_z^2}$ is the total momentum. Inside the solenoid magnet of the effective length L, the beam matrix is

$$M_2 = \begin{bmatrix} 1 & \frac{p}{eB}\sin(\frac{eB_zL}{p}) & 0 & \frac{p}{eB}(1-\cos(\frac{eB_zL}{p})) \\ 0 & \cos(\frac{eB_zL}{p}) & 0 & \sin(\frac{eB_zL}{p}) \\ 0 & -\frac{p}{eB_z}(1-\cos(\frac{eB_zL}{p})) & 1 & \frac{p}{eB}\sin(\frac{eB_zL}{p}) \\ -\sin(\frac{eB_zL}{p}) & 0 & 0 & \cos(\frac{eB_zL}{p}) \end{bmatrix}. \tag{2.100}$$

Similar to equation (2.99), the beam matrix at the exit edge of the solenoid magnet is

$$M_3 = \begin{bmatrix} 1 & 0 & 0 & 0 \\ 0 & 1 & -\frac{eB_z}{2p} & 0 \\ 0 & 0 & 1 & 0 \\ \frac{eB_z}{2p} & 0 & 0 & 1 \end{bmatrix}. \tag{2.101}$$

For the whole solenoid magnet, the product of the three matrices $M = M_1M_2M_3$ gives the final beam transport matrix, which is

$$
M = \begin{bmatrix}
\cos^2(\theta/2) & \dfrac{\sin(\theta/2)\cos(\theta/2)}{eB_z/2p} & \sin(\theta/2)\cos(\theta/2) & \dfrac{\sin^2(\theta/2)}{eB_z/2p} \\
\dfrac{-eB_z\sin(\theta/2)\cos(\theta/2)}{2p} & \cos^2(\theta/2) & \dfrac{-eB_z\sin 2(\theta/2)}{2p} & \sin(\theta/2)\cos(\theta/2) \\
-\sin(\theta/2)\cos(\theta/2) & \dfrac{-\sin^2(\theta/2)}{eB_z/2p} & \cos^2(\theta/2) & \dfrac{\sin(\theta/2)\cos(\theta/2)}{eB_z/2p} \\
\sin 2(\theta/2) & -\sin(\theta/2)\cos(\theta/2) & \dfrac{-eB_z\sin(\theta/2)\cos(\theta/2)}{2p} & \cos^2(\theta/2)
\end{bmatrix}
$$

.

Here $\theta = eB_z L/p$ and L is the solenoid effective length. The thin lens approximation is applied to the beam matrix by estimating that the length L and θ are small. Therefore, the beam matrix becomes [28]

$$
M = \begin{bmatrix}
1 & 0 & 0 & 0 \\
-\dfrac{1}{f} & 1 & 0 & 0 \\
0 & 0 & 1 & 0 \\
0 & 0 & -\dfrac{1}{f} & 1
\end{bmatrix}, \qquad (2.102)
$$

where f is the focal length of the solenoid magnet, which is given by [28]

$$
\frac{1}{f} = kL = \left(\frac{eB_z}{2p}\right)^2 L\,. \qquad (2.103)
$$

From equation (2.103), it is found that the focal length of the solenoid magnetic field relates to energy of the particle. Therefore, the electrons in the beam with energy spread are focused in different positions due to different solenoid magnetic focal lengths.

2.4 Transverse Phase Space and Beam Emittance

The electron beam quality depends greatly on electron distributions in transverse and longitudinal phase spaces. The longitudinal phase space is determined by the electron bunch length and the energy spread within the bunch. For the KU compact THz-FEL, the longitudinal properties can be modified by using a magnetic bunch compressor in a form of chicane magnet. Contradictory, the transverse phase space depends significantly on an intrinsic property called a transverse beam emittance, which can only be optimized from an electron injector system. Thus, the beam emittance is one of the most important properties to determine the quality of the RF electron gun. It is related to a relationship between transverse positions and angular displacements of electrons inside the transverse phase space, which can be explained by a phase ellipse occupied by electrons as shown in Fig. 2.11.

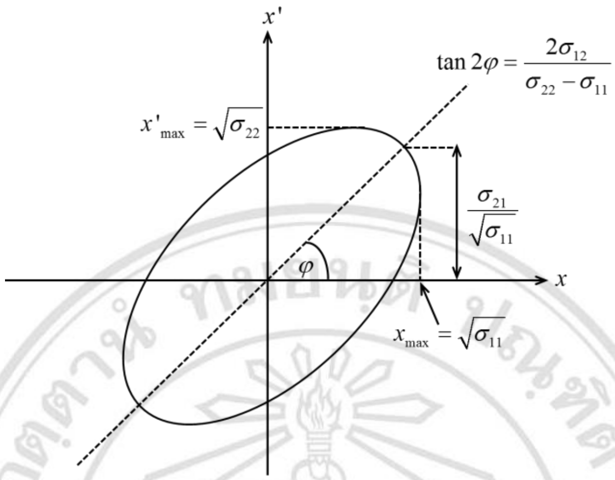

Figure 2.11: Ellipse phase space of the electron beam [29].

The transverse beam emittance ε is determined by an enclosed area of the phase ellipse shown in Fig. 2.11 as

$$\pi ab = \pi\varepsilon \ , \tag{2.104}$$

where a and b are the half-lengths of the ellipse major axis and minor axis, respectively. The phase ellipse and its orientation can be explained by using the beam emittance ε and the beam matrix parameters, which are σ_{11}, σ_{12}, σ_{21} and σ_{22}. Regarding to the ellipse phase space in Fig. 2.11, $\sqrt{\sigma_{11}}$ equals to half of the beam width, $\sqrt{\sigma_{22}}$ equals to half of the beam divergence while σ_{12} and σ_{21} describe the correlation between x and x'.

Here, the angular displacements are $x' \approx p_x / p_z$ and $y' \approx p_y / p_z$. The parameter p_z is the momentum of the electron in z-axis, which can be estimated to be $p_z \approx p$ when the transverse momenta $p_x << p_z$ and $p_y << p_z$. The beam matrix is then written as

$$\sigma = \begin{bmatrix} \sigma_{11} & \sigma_{12} \\ \sigma_{21} & \sigma_{22} \end{bmatrix}. \tag{2.105}$$

The transverse beam size is related to the rms transverse size and rms divergence. Then, an rms emittance can be calculated from the positions and the angular displacements of electrons as [30]

$$\varepsilon_{x,rms} = \sqrt{\langle x^2 \rangle \langle x'^2 \rangle - \langle xx' \rangle^2} \quad \text{and} \quad \varepsilon_{y.rms} = \sqrt{\langle y^2 \rangle \langle y'^2 \rangle - \langle yy' \rangle^2} \,. \tag{2.106}$$

In term of the beam matrix, the emittance is

$$\varepsilon = \sqrt{\det \sigma}. \tag{2.107}$$

An average momentum of the electron beam can be evaluated from the average beam energy $(E_{total})_{avg}$ by using the following equation

$$cp_{avg} = \beta (E_{total})_{avg} , \tag{2.108}$$

where $\beta = v / c$, v is the electron velocity and c is the speed of light. The total energy (E_{total}) is obtained from

$$(E_{total})_{avg} = \gamma m_0 c^2 = m_0 c^2 + KE_{avg} , \tag{2.109}$$

where m_0c^2 is the electron rest mass energy and γ is the Lorentz factor, $\gamma = 1/\sqrt{1-(v^2/c^2)}$. For comparison of electron beams produced from different accelerators with different energies, a normalize emittance ε_n is introduced to normalize the energy term from the emittance formula and is given by the following equation

$$\varepsilon_n = \beta\gamma\varepsilon_{rms} . \tag{2.110}$$

The vector of an electron at any position in the accelerator is defined by

$$X = \begin{bmatrix} x \\ x' \end{bmatrix}. \tag{2.111}$$

2.4.1 Quadrupole Scan Method

In this study, emittance measurement was performed by using the quadrupole scan method. The principle of this method is to measure the electron rms transverse beam size dependence on the quadrupole magnetic gradient. The measurement system consists of a quadrupole magnet, a drift space and a fluorescence screen. A schematic diagram of the experimental set-up for the quadrupole scan method is shown in Fig. 2.12.

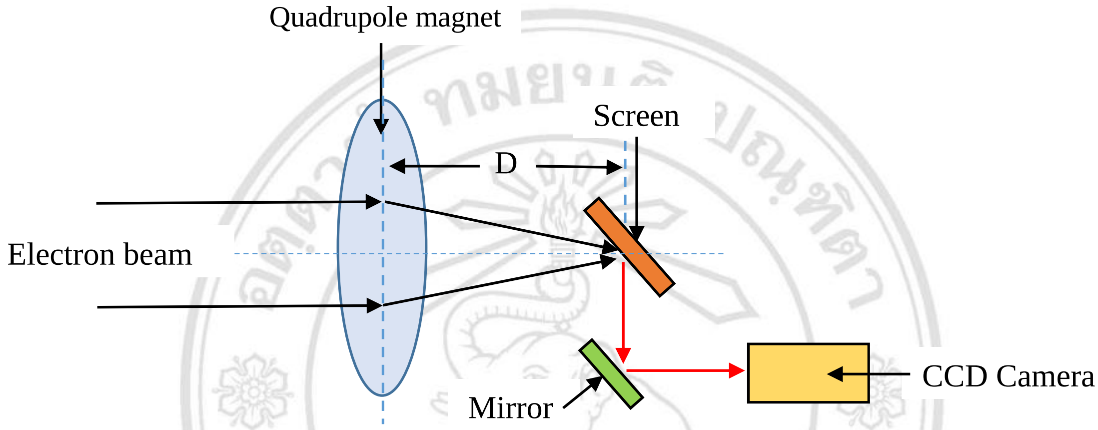

Figure 2.12: Schematic diagram of the experimental set-up for the quadrupole scan method.

Consider the components in the experimental set-up, let l is the effective length of the quadrupole magnet, D is a length of the drift space, which is the distance between the center of the quadrupole magnet and the view screen, σ_q and X_q are the beam matrix and the beam vector at the center of the quadrupole, while σ_s and X_s are the beam matrix and the beam vector at the screen. The matrix equations of the beam vectors at the center of the quadrupole magnet (q) and at the screen position (s) are [31]

$$X_q^T \sigma_q^{-1} X_q = 1, \tag{2.112}$$

and

$$X_s^T \sigma_s^{-1} X_s = 1. \tag{2.113}$$

Apply the transport matrix R to the beam matrix at the quadrupole magnet position, then the beam matrix at the screen position is

$$X_s = R X_q. \tag{2.114}$$

Replace X_s in equation (2.114) into equation (2.113), then equation (2.113) becomes

$$(RX_q)^T \sigma_s^{-1} (RX_q) = X_q^T R^T \sigma_s^{-1} R X_q = 1 . \tag{2.115}$$

Equations (2.112) is equal to equation (2.115), then we get

$$X_q^T R^T \sigma_s^{-1} R X_q = X_q^T \sigma_q^{-1} X_q . \tag{2.116}$$

$$\sigma_q^{-1} = R^T \sigma_s^{-1} R = R^T \sigma_s^T R^T \tag{2.117}$$

By using the invert relation, we get the beam matrix at the quadrupole positions

$$\sigma_q = R^{-1} \sigma_s (R^T)^{-1} . \tag{2.118}$$

Apply the matrices R and R^T to the left and the right hand side of the beam matrix σ_q in equation (2.118), then we get

$$R \sigma_q R^T = R R^{-1} \sigma_s (R^T)^{-1} R^T . \tag{2.119}$$

Therefore, the relationship between the beam matrices at the screen position and at the quadrupole position becomes

$$\sigma_s = R \sigma_q R^T . \tag{2.120}$$

There are four unknown parameters in the beam matrix σ_s, which are $(\sigma_s)_{11}$, $(\sigma_s)_{12}$, $(\sigma_s)_{21}$ and $(\sigma_s)_{22}$, where $(\sigma_s)_{12} = (\sigma_s)_{21}$. The only one parameter that we can directly measure is the transverse beam size at the screen, which is $(\sigma_s)_{11}$.

Properties of focusing and defocusing quadrupole magnets are equivalent to the properties of converging and divergent lens, respectively. Apply the thin lens approximation to the transport matrices of the quadrupole magnets in equations (2.92) and (2.93), which the length of the quadrupole magnet is considered to be very small compared to a focal length of the quadrupole. The approximations are [32]

$$\lim_{l \to 0} \left[\cos(\sqrt{k} l) \right] \to 1 , \qquad \lim_{l \to 0} \left[\cosh(\sqrt{|k|} l) \right] \to 1 ,$$

$$\lim_{l \to 0} \left[\frac{\sin(\sqrt{k} l)}{\sqrt{k}} \right] \to \frac{\sqrt{k} l}{\sqrt{k}} \to l \to 0 , \qquad \lim_{l \to 0} \left[\frac{\sinh(\sqrt{|k|} l)}{\sqrt{|k|}} \right] \to \frac{\sqrt{|k|} l}{\sqrt{|k|}} \to l \to 0 ,$$

$$\lim_{l\to 0}\left[-\sqrt{k}\sin(\sqrt{k}l)\right]\to\left[\sqrt{k}(\sqrt{k}l)\right]\to -kl\to -\frac{1}{f},$$

$$\lim_{l\to 0}\left[-\sqrt{|k|}\sinh(\sqrt{|k|}l)\right]\to\left[\sqrt{|k|}(\sqrt{|k|}l)\right]\to kl\to \frac{1}{f}.$$

Hence, the transport matrices of the focusing and defocusing thin quadrupole magnets are

$$M_{QF}=\begin{bmatrix}1&0&0&0\\-\frac{1}{f}&1&0&0\\0&0&1&0\\0&0&\frac{1}{f}&1\end{bmatrix}\quad\text{and}\quad M_{QD}=\begin{bmatrix}1&0&0&0\\\frac{1}{f}&1&0&0\\0&0&1&0\\0&0&-\frac{1}{f}&1\end{bmatrix}. \tag{2.121}$$

The relationship between the focal length and the strength of the quadrupole magnet can then be written as

$$\frac{1}{f}=\frac{qg}{p}l=kl, \tag{2.122}$$

Furthermore, the transport matrix of the drift space for transverse motion can be written as

$$M_D=\begin{bmatrix}1&D&0&0\\0&1&0&0\\0&0&1&D\\0&0&0&1\end{bmatrix}, \tag{2.123}$$

where D is the length of the drift space. For the components in the experimental set-up for the quadrupole scan method, the product of the matrices is $R=M_DM_{QF}$ or $R=M_DM_{QD}$. For convenience, the beam matrix of the quadrupole magnet is separated in two matrices corresponding to the x-axis and the y-axis. Thus, the dimensions of the matrix reduce from 4x4 to 2x2 and the matrix R is

$$R=\begin{bmatrix}1&D\\0&1\end{bmatrix}\begin{bmatrix}1&0\\-1/f&1\end{bmatrix}=\begin{bmatrix}1-D/f&D\\-1/f&1\end{bmatrix}=\begin{bmatrix}R_{11}&R_{12}\\R_{21}&R_{22}\end{bmatrix}. \tag{2.124}$$

From equation (2.120), the beam matrix at the screen position becomes

$$\sigma_s = \begin{bmatrix} R_{11} & R_{12} \\ R_{21} & R_{22} \end{bmatrix} \begin{bmatrix} (\sigma_q)_{11} & (\sigma_q)_{12} \\ (\sigma_q)_{21} & (\sigma_q)_{22} \end{bmatrix} \begin{bmatrix} R_{11} & R_{21} \\ R_{12} & R_{22} \end{bmatrix}. \tag{2.125}$$

The matrix element $(\sigma_s)_{11}$, which corresponds to $\langle x^2 \rangle$ or $\langle y^2 \rangle$, is calculated to be

$$(\sigma_s)_{11} = R_{11}^2(\sigma_q)_{11} + 2R_{11}R_{12}(\sigma_q)_{12} + R_{22}^2(\sigma_q)_{22},$$

$$(\sigma_s)_{11} = D^2(\sigma_q)_{11}\frac{1}{f^2} - 2D((\sigma_q)_{11} + D(\sigma_q)_{12})\frac{1}{f} + ((\sigma_q)_{11} + 2D(\sigma_q)_{12} + D^2(\sigma_q)_{22}), \tag{2.126}$$

Equation (2.126) suggests that the transverse beam size is a function of the focal length of the quadrupole magnet with a quadratic relation. The transverse beam size in x-axis or y-axis can be obtained from the Gaussian fitting of the histogram of the particle distribution. An example of the simulated transverse distribution of the electron beam is shown in Fig. 2.13. An example of the histogram and the Gaussian fitting of the simulated transverse distribution are shown in Fig. 2.14.

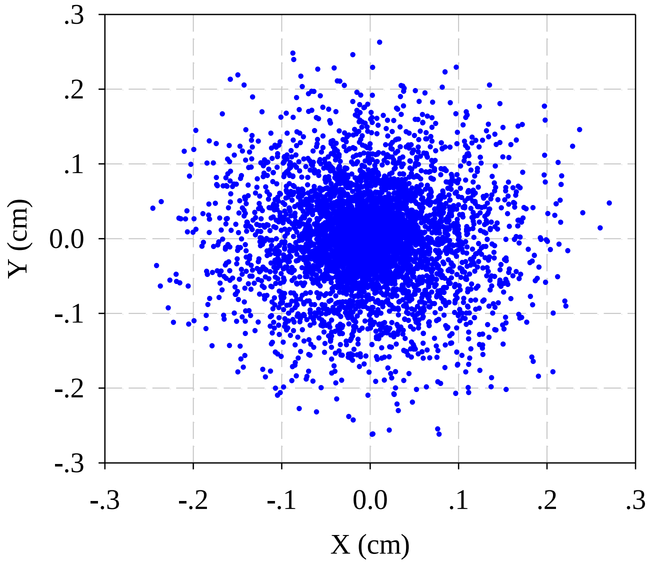

Figure 2.13: Example of simulated transverse distribution of the electron beam.

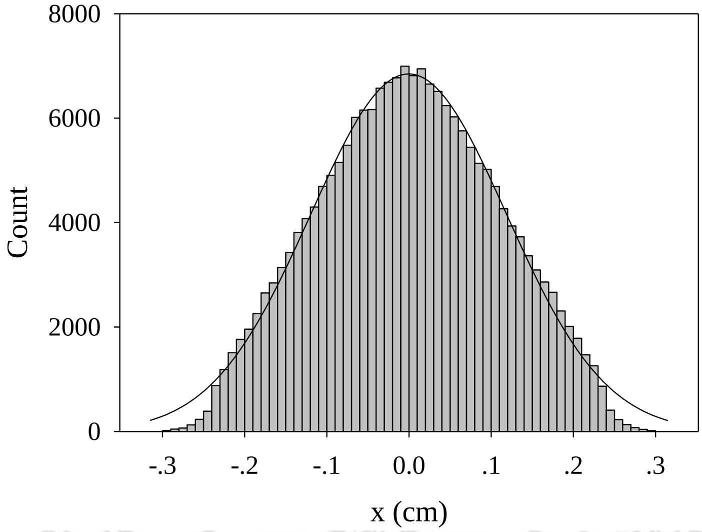

Figure 2.14: Example of histogram and the Gaussian fitting for the horizontal distribution of the beam.

In the quadrupole scan method, the transverse beam image is measured while adjusting the quadrupole magnetic gradient. Then, the transverse beam size is calculated for each gradient. For a Gaussian beam, the transverse beam size, which is achieved from the Gaussian fitting, is equal to an rms transverse beam size. Therefore, the rms transverse beam size can be defined as

$$\sigma_{x,rms} = \sqrt{\langle x^2 \rangle} \quad \text{and} \quad \sigma_{y,rms} = \sqrt{\langle y^2 \rangle}\,. \tag{2.127}$$

An example of the transverse beam size as a function of the focal length of the quadrupole magnet is shown in Fig. 2.15. The relation is fitted with a quadratic function in order to compare with the result of the beam matrix transportation as shown in equation (2.126). The fitting results is in form of

$$\sigma_{rms}^2 = A\frac{1}{f^2} + B\frac{1}{f} + C\,, \tag{2.128}$$

where σ is the transverse beam size in x-axis or y-axis, *f* is the focal length of the quadrupole magnet and the constants *A*, *B* and *C* are the fitting coefficients. Compare the fitting coefficients in equation (2.128) with the coefficients in equation (2.126) to obtain the values of the beam matrix elements $(\sigma_q)_{11}$, $(\sigma_q)_{12}$, $(\sigma_q)_{21}$ and $(\sigma_q)_{22}$ at the quadrupole magnet position. The beam matrix at the quadrupole magnet position is

$$(\sigma_q) = \begin{bmatrix} (\sigma_q)_{11} & (\sigma_q)_{12} \\ (\sigma_q)_{21} & (\sigma_q)_{22} \end{bmatrix}. \quad (2.129)$$

Thus, the beam emittance at the quadrupole magnet position can be calculated from

$$\varepsilon_{rms} = \sqrt{\det(\sigma_q)}\ . \quad (2.130)$$

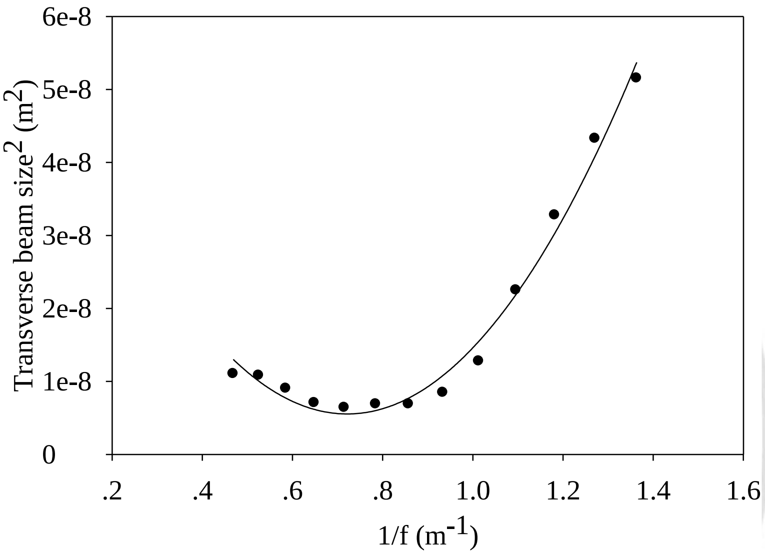

Figure 2.15: Example of relationship between the transverse beam size squared and the focal length (*f*) of the quadrupole magnet.

2.5 Space Charge Effect

The space charge effect is related to the electron cloud self-generated fields and forces in a space region. Consider two static identical charged particles with a charge of q as shown in Fig. 2.16. The Coulomb force causes a repulsing force between the two identical charged particles. If these particles travel with a velocity of $v = \beta c$, their behaviors are similar to two parallel currents. The currents generate magnetic fields, which produce the magnetic forces acting on the two parellel currents as shown in Fig. 2.16.

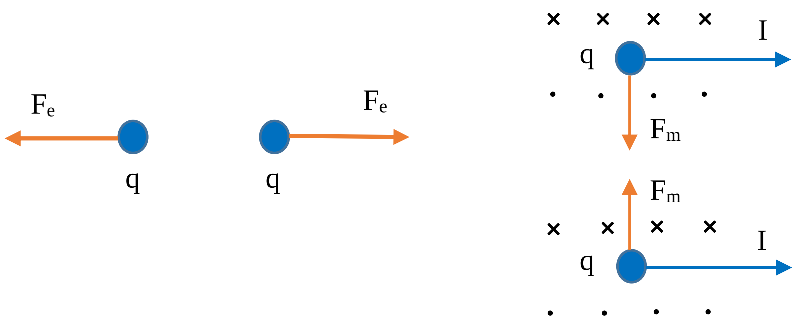

(a) (b)

Figure 2.16: (a) Coulomb forces between two static identical charged particles. (b) Magnetic forces between two parallel currents.

The idea of two static identical charged particles is extended to a group of static charged particles and a group of moving charged particle beam. For the group of static charged particles, the Coulomb force pushes the test particle outward. In case of the group of moving charged particles, the behavior is similar to many parallel currents inside the beam. The magnetic force due to the induced magnetic field from the parallel currents introduces the radial attractive force to the test particle. Diagrams of the repulsing force due to the electric field between the static identical particles and the attractive force due to the induced magnetic field for the parallel currents inside the beam are shown in Fig. 2.17.

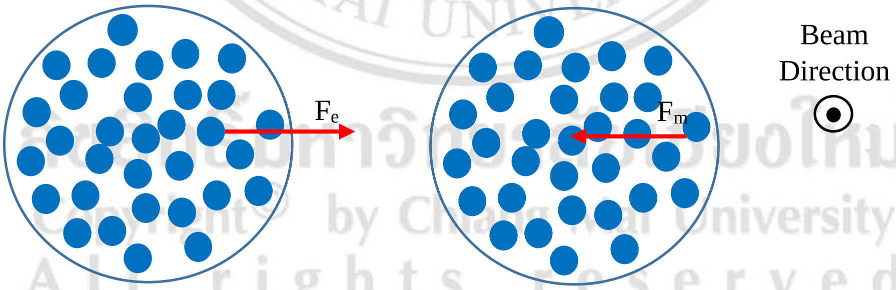

(a) (b)

Figure 2.17: (a) Coulomb electric repulsing force (F_e) on the test particle in a group of static charged particles. (b) The attractive magnetic force (F_m) on the test particle in the group of moving charged particles.

Consider a Gaussian beam with a standard deviation of σ_r and a radial charge density of

$$\rho(r) = \rho_0 \exp\left(\frac{-r^2}{2\sigma_r^2}\right), \tag{2.131}$$

where ρ_0 is the maximum charge density. The charge per unit length of the cylindrical beam is defined as

$$\lambda = 2\rho_0 \pi \sigma_r^2. \tag{2.132}$$

Consider a region where $0 < r \le R$, the radial electric field can be obtained by using Gauss's law as

$$\oiint_S \vec{E} \cdot d\vec{a} = \frac{1}{\varepsilon_0}\int_V \rho dV = \frac{1}{\varepsilon_0}\int_0^r 2\pi r l \rho(r) dr,$$

$$E_r(r) = \frac{\rho_0}{\varepsilon_0 r}\int_0^r \exp\left(\frac{-r^2}{2\sigma_r^2}\right) r dr = \frac{\rho_0}{\varepsilon_0 r}\frac{\sigma_r^2}{2}\left(1 - \exp(-r^2/2\sigma_r^2)\right). \tag{2.133}$$

Furthermore, the azimuthal magnetic field can be obtained by using Ampere's law as

$$\oiint_C \vec{B} \cdot d\vec{l} = \mu_0 \int \vec{J} \cdot d\vec{S} = \mu_0 \int \rho \vec{v}_s \cdot d\vec{S} = \mu_0 v_s \int_0^r 2\pi r \rho(r) dr,$$

$$B_\varphi(r) = \frac{\mu_0 v_s}{r}\int_0^r \exp\left(\frac{-r^2}{2\sigma_r^2}\right) r dr = \frac{\mu_0 v_s \rho_0}{r}\frac{\sigma_r^2}{2}\left(1 - \exp(-r^2/2\sigma_r^2)\right). \tag{2.134}$$

Consider the Lorentz force from the electromagnetic fields, which are generated from the electron beam itself, we get

$$\vec{F} = \vec{F}_e + \vec{F}_m,$$

where $$\vec{F}_e = q\vec{E}_r,$$

and $$\vec{F}_m = q(\vec{v} \times \vec{B}) = q\begin{vmatrix} \hat{r} & \hat{\varphi} & \hat{s} \\ 0 & 0 & v_s \\ 0 & B_\varphi & 0 \end{vmatrix} = -qv_s B_\varphi \hat{r}.$$

The Lorentz force from the electric and the magnetic fields becomes

$$\vec{F} = \vec{F}_e + \vec{F}_m = qE_r(r)\hat{r} - qv_s B_\varphi(r)\hat{r}. \tag{2.135}$$

Thus, the space charge force of the Gaussian beam with the standard deviation of σ_r is

$$\vec{F} = q\frac{\rho_0}{\varepsilon_0 r}\frac{\sigma_r^2}{2}\left(1-\exp\left(\frac{-r^2}{2\sigma_r^2}\right)\right)\hat{r} - qv_s\frac{\mu_0 v_s \rho_0}{r}\frac{\sigma_r^2}{2}\left(1-\exp\left(\frac{-r^2}{2\sigma_r^2}\right)\right)\hat{r},$$

$$\vec{F} = \frac{q\rho_0\sigma_r^2}{2r}\left(\frac{1}{\varepsilon_0} - v_s^2\mu_0\right)\left(1-\exp\left(\frac{-r^2}{2\sigma_r^2}\right)\right)\hat{r}. \tag{2.136}$$

Here, $v_s^2 = \beta^2 c^2$ and $\mu_0 = 1/\varepsilon_0 c^2$. Therefore, the space charge force is

$$\vec{F} = \frac{q\rho_0\sigma_r^2}{2\varepsilon_0 r}\left(1-\beta^2\right)\left(1-\exp\left(\frac{-r^2}{2\sigma_r^2}\right)\right)\hat{r},$$

$$\vec{F} = \frac{q\rho_0\sigma_r^2}{2\varepsilon_0 r\gamma^2}\left(1-\exp\left(\frac{-r^2}{2\sigma_r^2}\right)\right)\hat{r}. \tag{2.137}$$

According to the above equation, the space force introduces a defocusing effect, which is inversely proportional to the beam energy $\gamma = E_{total}/m_0c^2$. Besides the beam energy, it also depends on the charge distribution or the charge density of the beam.

2.6 Stopping Power of Materials

Generally, the beam energy measurement is performed in a vacuum chamber, where the electron beam travels through the accelerator system without hitting any particle. In this case, the electron beam does not lose its energy. Unfortunately, during this study the beam energy measurement was performed in air due to the equipment limitation. The vacuum chamber at the end of the accelerator is closed by a beam extraction window in order to keep the vacuum condition inside the accelerator. After the electron beam hits the extraction window, it then travels in air. When hitting on the extraction window and other particles such as molecules of gas or vapor water, the beam loses its energy. Therefore, the study on the energy loss of the beam when it travels in matter is important for the beam energy measurement.

A stopping power in materials is defined as a decelerating force that acts on a charged particle when it travels in the matter. This results in the energy loss of the particle. The stopping power depends on the initial energy of the particle, the particle type and the material properties. The stopping power of the particle in any material equals to the energy lost per unit path length (x), which is

$$S(E) = -\frac{dE}{dx}. \tag{2.138}$$

When the charged particle travels through the material, the retarding force increases until it reaches the end of the traveling length. Then, the particle energy rapidly drops to zero. This relationship is called the Bragg curve and the maximum point is called the Bragg peak [33]. Equation (2.138) defines a linear stopping power, which is usually introduced in a unit of MeV/cm. A mean moving path of the charged particle inside the material can be obtained by integrating the stopping power over the particle energy, which is [34]

$$R_{CSDA} = \int_0^{E_0} \frac{1}{S(E)} dE = \int_0^{E_0} \left(\frac{dx}{dE}\right) dE, \tag{2.139}$$

where R_{CSDA} is the continuous slowing down approximation (CSDA) range in unit of g/cm^2, $S(E)$ is the linear stopping power and E_0 is the initial energy of the charged particle. The R_{CSDA} defines the path length of the charged particle that travels with slowing-down velocity until it stops inside the material.

The stopping power can be categorized into three kinds, which are an electronic, a nuclear and a radiative stopping powers. The electronic stopping power $S_e(E)$ is related to an inelastic collision between the moving charged particles and bounded electrons in the material structure. The energy that transfers from the incident charged particle can be a cause of the ionization or the change of the bounded electron orbit. It causes the slowing-down process of the charged particle in the material. The nuclear stopping power $S_n(E)$ is related to the elastic collisions between the charged particles and nuclei in the material. A probability of the collision between the charged particle and the material nuclei increases when the charged particle has slowed down. The amount of the electronic and nuclear stopping powers is called the collision stopping power. In case of charged particles with high energies, the radiative stopping power $S_{rad}(E)$ is related to the bremsstrahlung emission, which occurs when the charged particle travels through the material. Therefore, the total stopping power of the material can be written as the sum of these three stopping powers.

$$S_{tot}(E) = S_e(E) + S_n(E) + S_{rad}(E)\,, \tag{2.140}$$

Since, the collision stopping power $S_{col}(E)$ is the sum of the electric and the nuclear stopping powers, the total stopping power becomes

$$S_{tot}(E) = S_{col}(E) + S_{rad}(E)\,, \tag{2.140}$$

An energy loss (E_{loss}) of the charged particle in the material can be calculated from

$$E_{loss} = S_{tot}(E)\rho d\;, \tag{2.141}$$

where ρ is the material density and d is the material thickness. The total stopping power, the material density and the material thickness usually are introduced in units of MeV cm^2/g, g/cm^3 and cm, respectively.